BORRMANN TOPOGRAPHIC INVESTIGATION ON DISLOCATION CONFIGURATION IN WELL-ANNEALED AND LIGHTLY DEFORMED COPPER CRYSTALS

A. Merlini, F.W. Young

BORRMANN TOPOGRAPHIC INVESTIGATION ON DISLOCATION CONFIGURATION IN WELL-ANNEALED AND LIGHTLY DEFORMED COPPER CRYSTALS (1)

A. MERLINI(2) and F. W. YOUNG, Jr.

Solid State Division, Oak Ridge National Laboratory Oak Ridge, Tennessee U.S.A.

Résumé. — On a étudié, par la méthode de topographie aux rayons X de Borrmann, les dislocations dans des cristaux de cuivre bien recuits et légèrement déformés. On a déterminé, par observation stéréoscopique et par analyse vectorielle des topographies, la disposition des lignes dans l'espace. On a obtenu les vecteurs de Burgers par application des conditions du contraste nul si $\boldsymbol{g}.\boldsymbol{b} = 0$ et $\boldsymbol{b}.(\boldsymbol{g} \times \boldsymbol{n}) = 0$. Les résultats sont en accord avec l'hypothèse $\boldsymbol{b} = \langle 110 \rangle$. On n'a pas observé de dislocations vis, et peu de dislocations coins dans les cristaux recuits, et elles ne se trouvaient souvent pas dans les plans $\{111\}$, ou suivant des directions cristallographiques simples. On en a déduit que la montée était très importante pour établir leur répartition. Les dislocations vis dominaient dans le cristal légèrement déformé. Le contraste relatif de dislocation et les largeurs d'image ont été comparées à $\frac{|\boldsymbol{g}.\boldsymbol{b}|}{|\boldsymbol{g}|\,|\boldsymbol{b}|}$ et $\frac{|\boldsymbol{g} \times \boldsymbol{n}|}{|\boldsymbol{g}|}$, pour les dislocations fraîches et anciennes des deux types. Bien qu'on ait trouvé dans quelques cas une corrélation relative, il a paru évident que d'autres facteurs que les deux quantités ci-dessus influent de façon importante sur la largeur d'image et le contraste.

Abstract. — An investigation of the dislocations in well-annealed and lightly deformed copper crystals was made with Borrmann x-ray topography. The spatial arrangements of the lines were determined by stereoscopic views and by a vector analysis of the topographs. Burgers vectors were determined by application of the conditions of no contrast if $\boldsymbol{g}.\boldsymbol{b} = 0$ and $\boldsymbol{b}.(\boldsymbol{g} \times \boldsymbol{n}) = 0$. The results were consistent with the hypothesis that $\boldsymbol{b} = \langle 110 \rangle$. No pure screw and few pure edge dislocations were observed in the annealed crystals, often the dislocations did not lie on $\{111\}$ planes or along simple crystallographic directions. It was concluded that climb was very important in establishing the dislocation configuration. Screw dislocations were prevalent in the lightly deformed crystal. Relative dislocation contrast and image widths were compared with

$$\frac{|\boldsymbol{g}.\boldsymbol{b}|}{|\boldsymbol{g}|\,|\boldsymbol{b}|} \text{ and } \frac{|\boldsymbol{g} \times \boldsymbol{n}|}{|\boldsymbol{g}|}$$

for both fresh and aged dislocations of all types. Although in some cases there was a qualitative correlation, it was clear that other factors than the above two quantities were important for the determination of image width and contrast.

Introduction. — Since the original discovery that individual dislocations could be made visible within the interior of crystals by X-ray diffraction contrast, topographic techniques became a powerful means to investigate dislocation configurations in a variety of crystals of low dislocation density. Many crystals, such as diamond, silicon, calcite, aluminium and iron – 3 % silicon were studied by the transmission method developed by Lang [1]. However, this technique, limited to thin crystals, renders specimen preparation very difficult in the case of crystals made of heavy elements which greatly absorb the wavelengths used in X-ray diffraction.

The growth and preparation of copper crystals of low dislocation density renewed interest in the application of topography in anomalous transmission (Borrmann topography) to the study of dislocations in metal crystals. The results of an earlier investigation of dislocations in copper was reported elsewhere [2]. Since then the resolution of Borrmann topographs has been considerably improved and a method for making stereo pairs has been devised [3].

The present work is a detailed study of the spatial

(1) Research sponsored by the U. S. Atomic Energy Commission under contract with Union Carbide Corporation.

(2) Solid State Physics, Euratom C. C. R., Ispra, Italy.

configuration of the dislocations in annealed and lightly deformed crystals of copper. Some aspects of the contrast associated with the dislocations were also investigated in an attempt to learn the important factors involved in the diffraction contrast found in Borrmann topography.

Experimental. — A crystal 2.5 cm diameter by 15 cm was grown from 99.999 % copper as described previously [4] with the unseeded growth direction approximately [30$\bar{4}$]. A parallelepiped 1 × 1 × 2 cm with 1 × 2 cm face (10$\bar{1}$) was acid sawed from this crystal, then annealed at 1075 °C for two weeks. The dislocation density was not monitored during this treatment. (It has been demonstrated that little or no deformation is introduced by the acid sawing [5] and that the anneal serves to reduce the dislocation density resulting from growth and/or handling [4]). The parallelepiped was irradiated with 10^{17}/cm^2 fast neutrons in order to pin the dislocations, then acid sawed into lamellæ 1 × 1 × t cm ($0.03 \leqslant t \leqslant .15$) with the 1 × 1 cm face (111). The (111) surfaces were acid polished, electropolished and etched with a dislocation etch [4]. Two of these lamellæ were heavily deformed in one corner then re-annealed at 1075 °C. They were accidentally deformed very lightly in the main part of the lamellæ sometime during this anneal and the subsequent mounting.

The lamellæ were examined with Borrmann X-ray topography as described previously [3]. The orientation of the lamellæ is shown in figure 1 ; $\bar{1}1\bar{1}$, $\bar{1}\bar{1}1$ and $1\bar{1}\bar{1}$ topographs, including stereo pairs, were taken routinely of the entire lamellae and appropriate 202, 200, 113 and 222 topographs were taken of portions of the lamellæ to make positive identification of certain defects and of their location. Topographs for which the X-rays exit from ($\bar{1}\bar{1}\bar{1}$) are denoted plus ; from (111), minus. In addition, the positions of dislocation-surface intersections were monitored as etch pits, but this evidence is not presented here.

Results. — All the lamellæ had very similar dislocation arrangements, with the exception that one sub-boundary (angle of misorientation only a few seconds) was observed in two of the lamellæ from one end of the parallelepiped. Therefore one of the lamellæ about 0.034 cm thick, which did not contain the sub-boundary, is described in detail as representative. Since the neutron irradiation only served to maintain the dislocations in the exact positions they occupied in the parallelepiped, this lamella is referred to as annealed. Similarly, one of the reannealed, then slightly deformed lamellæ about 0.045 cm thick is described and referred to as deformed.

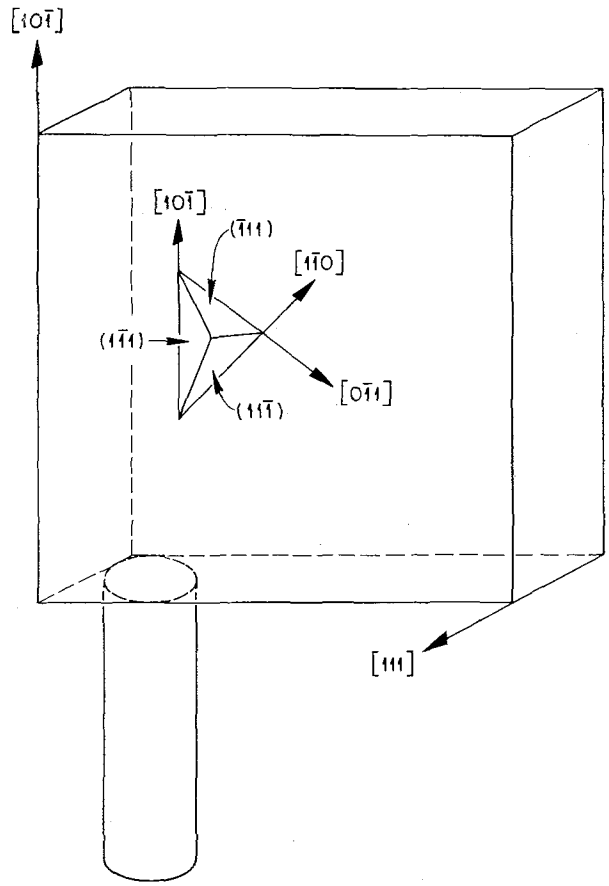

FIG. 1. — Diagram of the Crystallography of the Lamellae.

A $\bar{1}1\bar{1}$ plus topograph of the annealed lamella and a key identifying some of the dislocations are shown in figure 2. A stereo pair of $\bar{1}1\bar{1}$ is shown in figure 3 at lower magnification. (The prints are positives, i. e., black areas on the prints correspond to areas of decreased intensity on the X-ray plate). The average dislocation density N as determined by etch pit count on (111) and ($\bar{1}\bar{1}\bar{1}$) was 2.7×10^3/cm^2. Approximately the same value for N would be deduced from these topographs.

The Burgers vectors were determined by applying the conditions, no contrast if $\boldsymbol{g}.\boldsymbol{b} = 0$ and if $\boldsymbol{b}.(\boldsymbol{g} \times \boldsymbol{n}) = 0$ ($\boldsymbol{g}$ = diffraction vector ; $\boldsymbol{b}$ = Burgers vector ; $\boldsymbol{n}$ = unit vector lying along dislocation line). To determine $\boldsymbol{n}$, the projection direction $\boldsymbol{P}_i$ of the dislocation was determined in at least two topographs. Then $\boldsymbol{P}_i \times \boldsymbol{r}_i = \boldsymbol{V}_i$ ($\boldsymbol{r}_i$ = direction of propagation of X-rays inside the crystal for each $\boldsymbol{P}_i$) ; and $\boldsymbol{V}_i \times \boldsymbol{V}_j = \boldsymbol{n}$. Obviously, some rule of rational indices need be applied ; it is estimated that the error in the direction of $\boldsymbol{n}$ is $\pm$ 3°. On application of the above conditions for

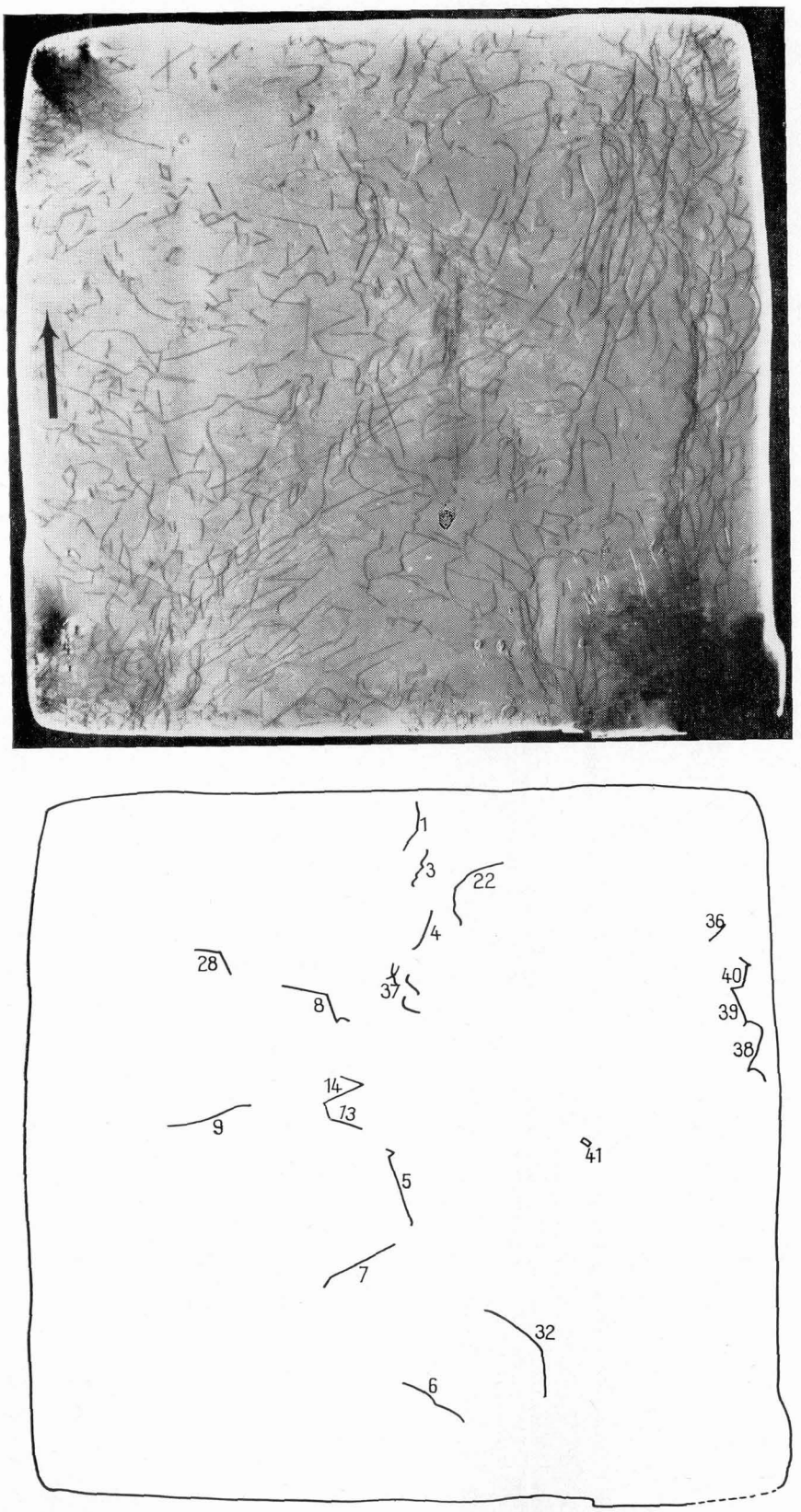

FIG. 2. — *a*) $\bar{1}1\bar{1}$ Plus topograph of annealed lamella. Edge of lamella is 1 cm. Mo radiation. Arrow indicates $[10\bar{1}]$. *b*) Key to dislocations described in Table II.

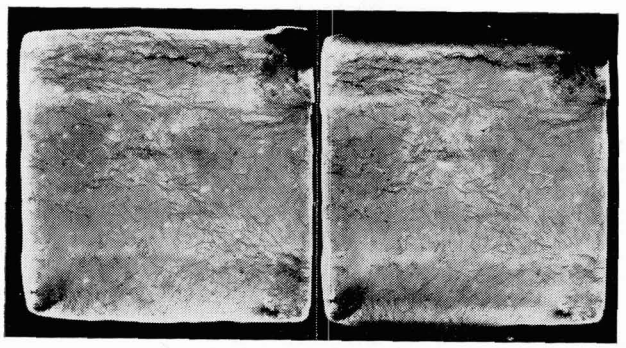

FIG. 3. — A $\bar{1}1\bar{1}$ Stereo Pair of Lamella of figure 2 (This pair can best be viewed with the aid of two converging lens with a planar separation of about 6 cm). Ag radiation.

contrast to those topographs we have found no results which are inconsistent with hypothesis that $\boldsymbol{b} = \langle 110 \rangle$. Burgers vectors of types $\langle 100 \rangle$ or $\langle 111 \rangle$ can definitely be eliminated, while vectors of higher indices are highly improbable from energy arguments.

In general, the dislocations are imaged as black lines in the prints, but sometimes they appear as black and white lines or even as white lines. We have called these latter two cases " anomalous contrast " ; it

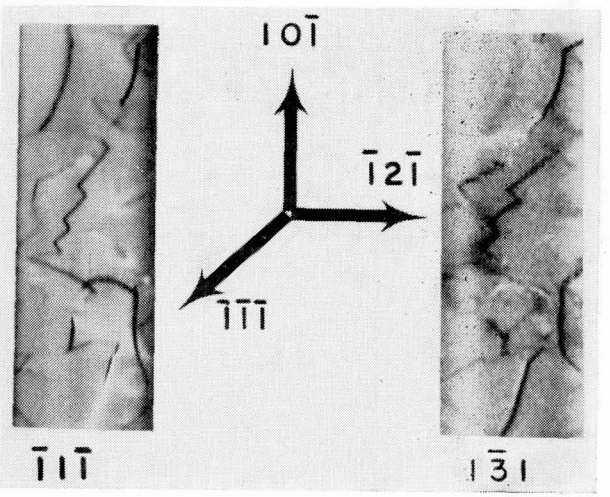

FIG. 4. — $\bar{1}1\bar{1}$ and $\bar{1}31$ Topographs of the region of the annealed lamella containing dislocation 3. Ag radiation.

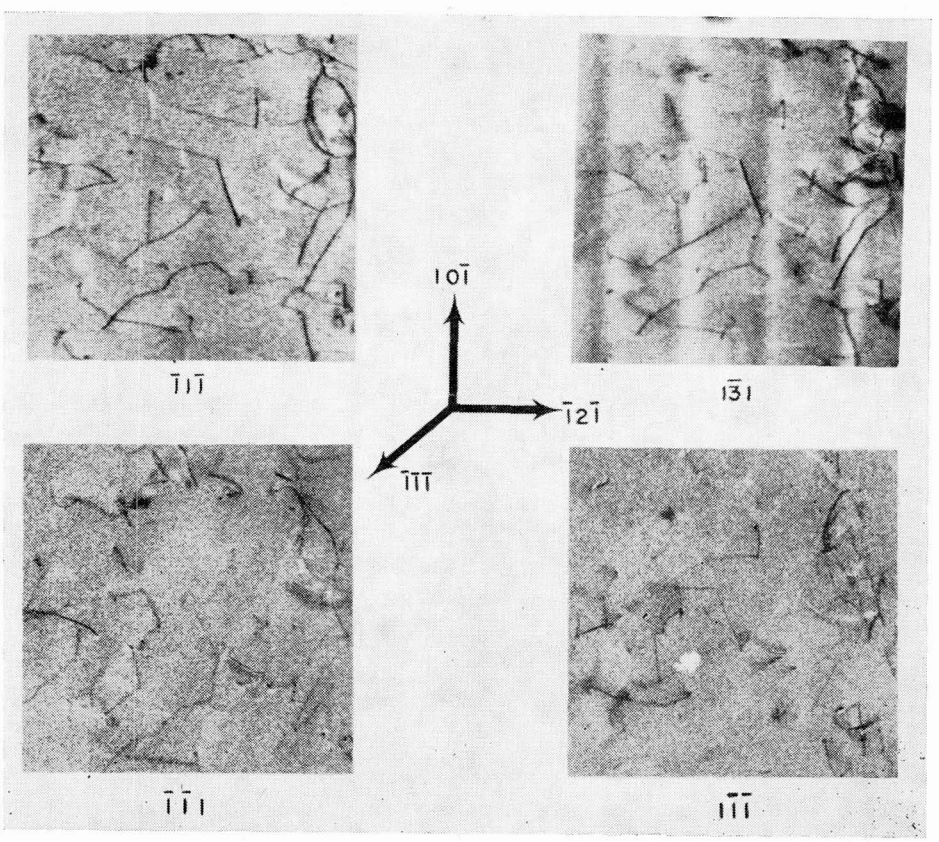

FIG. 5. — $\bar{1}1\bar{1}$, $1\bar{3}1$, $\bar{1}\bar{1}1$ and $1\bar{1}\bar{1}$ Topographs of the region of the annealed lamella containing dislocation 8. Ag radiation.

reverses between the diffracted and transmitted Borrmann beams. Anomalous contrast was seen only for dislocations which lay near either surface, the amount of such contrast was an inverse function of the distance from the surface, and strong anomalous contrast was only observed for edge dislocations or for mixed dislocations with strong edge character. Lang [1] reported that this type of contrast can be used to determine the sense of $\boldsymbol{b}$ in thin crystal topography. We have not yet demonstrated a similar correspondence for Borrmann topography.

A number of dislocations were analyzed completely. Dislocation 3, see figure 2, is a zig-zag line. It was observed in $\bar{1}1\bar{1}$ and $1\bar{3}1$, not observed in $\bar{1}\bar{1}1$ or $1\bar{1}\bar{1}$ topographs. Therefore $\boldsymbol{b} = [101]$. Enlargements of the portions of $\bar{1}1\bar{1}$ and $1\bar{3}1$ topographs containing this dislocation are shown in figure 4. For the longer A segments $\boldsymbol{P}_{\bar{1}1\bar{1}} = [12\bar{3}]$ and $\boldsymbol{P}_{1\bar{3}1} = [16\bar{7}]$; therefore $\boldsymbol{n} = [\bar{1}\bar{2}1]$ and these are pure edge components lying in (111). The shorter B segments have approximately the same projected directions in both topographs ; therefore $\boldsymbol{n} = \boldsymbol{P} = [3\bar{1}\bar{2}]$ and the plane containing both $\boldsymbol{b}$ and $\boldsymbol{n}$ is $(15\bar{1})$, which is not a glide plane. We conclude that this dislocation must have climbed some to assume its present configuration. Several topographs of portions of the crystal containing dislocation 8 are shown in figure 5. From the stereo pair it can be seen that the darker segment A lies near $(\bar{1}\bar{1}\bar{1})$, while the other segment B extends through the crystal. Although there is a faint image of segment A in $\bar{1}\bar{1}1$, we conclude $\boldsymbol{b} = [\bar{1}10]$. Since for segment A, P is the same in all topographs, $\boldsymbol{n}_A = \boldsymbol{P} = [5\bar{2}\bar{3}]$. For B segment $\boldsymbol{P}_{\bar{1}1\bar{1}} = [\bar{2}31]$, $\boldsymbol{P}_{1\bar{1}\bar{1}} = \bar{5}94$; therefore $\boldsymbol{n}_B \cong 2\bar{1}1$. The plane containing $\boldsymbol{b}$ and $\boldsymbol{n}_A$ is (111), while $\boldsymbol{b}$ and $\boldsymbol{n}_B$ lie in $(11\bar{1})$. Thus segment A is in the cross glide plane of segment B, and it is possible that this dislocation is a glide form. Note that the angle between the two segments is $\approx 120°$ in the topographs, but this value is fortuitous. The angle between $\boldsymbol{b}$ and $\boldsymbol{n}$ is 36° and 30° for segments A and B respectively, indicating no obvious crystallographic significance for the particular configuration. In Table I $\frac{|\boldsymbol{g}.\boldsymbol{b}|}{|\boldsymbol{g}|\,|\boldsymbol{b}|}$ and $\frac{|\boldsymbol{g} \times \boldsymbol{n}_A|}{|\boldsymbol{g}|}$ are listed for the reflections used in figure 5 ([3]). Apparently there is qualitative agreement between the magnitude of these two quantities and the observed contrast, but closer inspection shows that the agreement is not quantitative. If the faint image seen in the $\bar{1}\bar{1}1$ topograph is used as the indication of the amount of contrast from $|\boldsymbol{g} \times \boldsymbol{n}_A|$, then the contribution from the cross product term cannot account for the difference in contrast between $\bar{1}1\bar{1}$ and $1\bar{1}\bar{1}$ topographs.

([3]) Since only relative comparisons are made, taking the unit vector $\boldsymbol{b}/|\boldsymbol{b}|$ instead of $\boldsymbol{b}$ appears to be justified. This justification is not valid « a priori » for $\boldsymbol{g}$ when topographs corresponding to reflections of different type are compared. However, the semiquantitative conclusions drawn in this work are not affected by using $\boldsymbol{g}/|\boldsymbol{g}|$ in the place of a vector $\boldsymbol{g}$ of proper magnitude.

TABLE I

$\boldsymbol{g}$	$\lvert \boldsymbol{g}.\boldsymbol{b} \rvert / \lvert \boldsymbol{g} \rvert \lvert \boldsymbol{b} \rvert$	$\lvert \boldsymbol{g} \times \boldsymbol{n}_A \rvert / \lvert \boldsymbol{g} \rvert$
$1\bar{1}\bar{1}$	.816	.35
$\bar{1}1\bar{1}$	.816	.93
$\bar{1}\bar{1}1$	0	.83
$1\bar{3}1$	.85	.92

Information on the dislocations numbered in figure 2 is presented in Table II ; they are representative of the dislocations seen in this topograph. From this table and from analysis of other dislocations not visible in $\bar{1}1\bar{1}$ topograph, we conclude :

1) There are no pure screw dislocations in this lamella.

2) There are a few pure edge dislocations, but most of the dislocations are mixed. Often $\boldsymbol{n}$ is not a simple crystallographic direction. Although the dislocation lines make many sharp angles, generally these angles have no crystallographic significance.

3) Many dislocations do not lie in { 111 } planes.

4) For dislocations bowed on a slip plane, the stress corresponding to the radius of curvature is about 1 g/mm^2.

5) The dislocation structure seen in this lamella could not have resulted from glide only. Therefore, climb (probably occurring during the high temperature anneal) was very important in establishing this quasi-equilibrium configuration.

It cannot be concluded that these dislocations would not act as sources in a subsequent deformation of this lamella. The resolution of the topographic method is not sufficient to rule out the possibility of dislocation segments 10-50 μ in length lying in the appropriate slip planes.

There are a few black spots of contrast in the several topographs. For crystals with $N \sim 10^2/\text{cm}^2$ the number of these spots is much greater, $\sim 10^5/\text{cm}^3$, and they have been ascribed to vacancy clusters of various forms [6].

TABLE II

Dislocation	b	n	$b \times n$	arc cos $\frac{b.n}{\lvert b \rvert \lvert n \rvert}$	Observations
1	$\bar{1}10$	$10\bar{1}$	111	60°	Bowed ; from radius, $\sigma < 1$ g/mm^2
3	101	A) $12\bar{1}$	$\bar{1}11$	90°	Zig Zag. Not a glide form
		B) $3\bar{1}\bar{2}$	$15\bar{1}$	79°	
4	$\bar{1}10$	$21\bar{3}$	~ 111	79°	From stereo, clearly not in (111)
5	$\bar{1}10$	$\bar{3}12$	111	40°	Length ≈ 1 mm
6	$0\bar{1}1$	~ $1\bar{1}0$-$10\bar{1}$	111	~ 60°-120°	Bowed ; at cusp $\sigma \approx 1$ g/mm^2
		~ $1\bar{1}0$-$\bar{3}21$	111	~ 60°- 80°	
7	101	~ $01\bar{1}$	~ $\bar{1}11$	60°	From stereo, clearly not in (111)
8	$\bar{1}10$	A) $5\bar{2}\bar{3}$	111	36°	Possibly a cross slip form
		B) $2\bar{1}1$	$11\bar{1}$	30°	
9	$\bar{1}10$	$01\bar{1}$	111	60°	
13	A) $\bar{1}10$	$5\bar{4}3$	$33\bar{1}$	26°	A complex of dislocations with some segments too short for analysis
	B) $\bar{1}10$	$2\bar{1}\bar{1}$	111	30°	
14	A) 101	$1\bar{7}6$	$7\bar{5}\bar{7}$	58°	
	B) 101	14, 1, 9	$\bar{1}51$	12°	
22	$\bar{1}10$	$11\bar{2}$-$01\bar{1}$	111	90°-60°	Bowed-edge on one end, 60° on other end
28	$0\bar{1}1$	$2\bar{1}\bar{1}$	111	90°	
32	$0\bar{1}1$	A) $7\bar{4}\bar{3}$	111	60°	Note that part C lies on cross slip plane, so this entire dislocation could be a glide form
		B) $5\bar{1}\bar{4}$	111	60°	
		C) 312	$\bar{1}11$	80°	
36	$\bar{1}10$	$\bar{3}\bar{7}4$	225	70°	
37	101	144	$\bar{4}\bar{3}4$	50°	
38	$0\bar{1}1$	No long straight portions	Not {111}	~ 45°	Another case where bowing is not in a slip plane. Complex dislocations. May be some helical form
39	$\bar{1}10$				
40	101				
41	101	A) $\bar{1}21$	111	90°	Rectangular loop. Not on a slip plane, not a condensed loop – can't explain origin
		B) $0\bar{1}4$	$\bar{1}41$	~ 45°	

The magnitudes of $|g.b|/|g||b|$ and of $b.(g \times n)|/|g||b|$ were determined for a large number of dislocations. There was no simple correlation between either one of these two magnitudes and the relative contrast of a dislocation image. In order to investigate more carefully the relation between $|g.b|$ and dislocation contrast, $\bar{1}1\bar{1}$, $02\bar{0}$, $\bar{2}0\bar{2}$, $\bar{1}3\bar{1}$, $\bar{2}2\bar{2}$ plus and $02\bar{0}$ minus topographs were made of one portion of the lamella and are shown in figure 6. For this series g. $[10\bar{1}] = 0$, so the orientation of a dislocation with respect to the vertical direction is unchanged. It appears that there is no simple correlation of the relative contrast of these dislocations with the magnitude of $|g.b|/|g||b|$. For example,

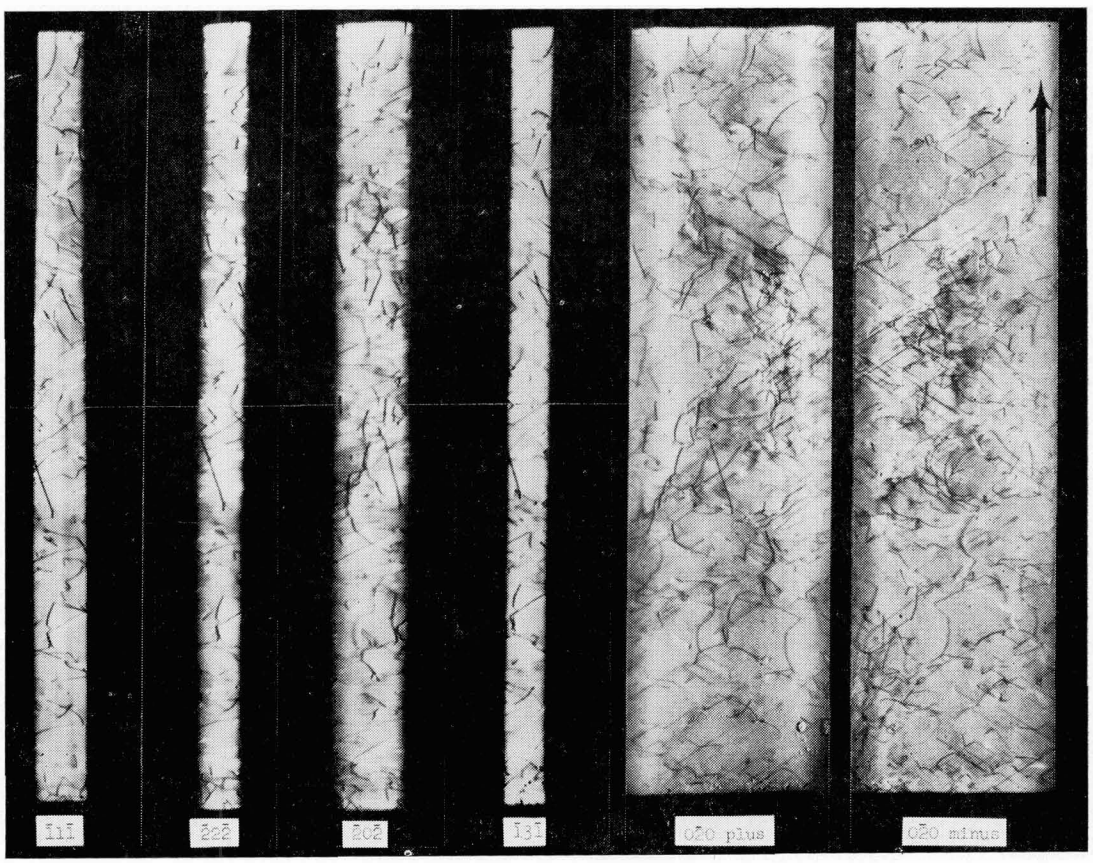

FIG. 6. — Different Topographs (all with $g.[10\bar{1}] = 0$) of one portion of the annealed lamella. Ag radiation.

TABLE III

		$\bar{1}1\bar{1}$		$02\bar{0}$		$\bar{2}0\bar{2}$		$1\bar{3}1$		$\bar{2}2\bar{2}$	
Disl.	b	$\frac{\lvert b.g\rvert}{\lvert g\rvert\lvert b\rvert}$	w	$\frac{\lvert b.g\rvert}{\lvert g\rvert\lvert b\rvert}$	w	$\frac{\lvert b.g\rvert}{\lvert g\rvert\lvert b\rvert}$	w	$\frac{\lvert b.g\rvert}{\lvert g\rvert\lvert b\rvert}$	w	$\frac{\lvert b.g\rvert}{\lvert g\rvert\lvert b\rvert}$	w
3	101	.82	10	0	10(*)	1	—	.43	10-12	.82	12.5-15
5	$\bar{1}10$	.82	10	.71	10-12	.5	20	.85	20	.82	18-20
7	101	.82	10	0	10-12.5 (*)	1	12.5	.43	12.5	.82	—
8	$\bar{1}10$	.82	9	.71	9-10	.5	10	.85	20	—	—

(*) Faint image.

for dislocations 5 and 8 $\boldsymbol{b} = [\bar{1}10]$, yet in the $\bar{2}0\bar{2}$ topograph 8 exhibits more contrast than 5, while in the other topographs both 5 and 8 exhibit more contrast than most of the other dislocations. Of particular interest is the fact that dislocations 3 and 7 appear in the $0\bar{2}0$ topographs though $\boldsymbol{g}.\boldsymbol{b} = 0$. By comparing the images in plus and minus topographs it was found that this contrast for 3 had essentially no component of anomalous contrast; for 7 it was anomalous contrast only. The relative amount of anomalous contrast is often greater in higher order topographs. Compare the $\bar{1}1\bar{1}$ and $\bar{2}2\bar{2}$ topographs; it is apparent that dislocations terminating in $(\bar{1}\bar{1}\bar{1})$ (the exit surface of X-rays) exhibit much greater anomalous contrast; in particular dislocations 37. In lieu of a quantitative method of determining contrast, image widths w where measured on the prints and values of $\frac{|\boldsymbol{g}.\boldsymbol{b}|}{|\boldsymbol{g}||\boldsymbol{b}|}$ and w are listed in Table III for several of the dislocations. It is concluded that there is no simple correlation between image width and $|\boldsymbol{g}.\boldsymbol{b}|$.

Plus $\bar{1}\bar{1}1$, $1\bar{1}\bar{1}$ and $\bar{1}1\bar{1}$ topographs of the deformed lamella are shown in figures 7*a*, 7*b* and 7*c*, respectively. This is the same crystal of figure 8 in ref. 2; it was subsequently thinned by electropolishing so that the dislocation structure changed slightly and the improved resolution of the present topographs allows much more information to be obtained. One corner of the lamella was so badly deformed that no useful information could be obtained by Borrmann topography, as shown in figure 7*b*. The dislocations labeled 1, 2 and 7, and those parallel to them, are screw with Burgers vectors $[\bar{1}01]$, $[0\bar{1}1]$ and $[\bar{1}10]$, respectively. They generally lie near the center of the lamella. It is apparent that they do not lie exactly along the directions of their Burgers vectors. In a 200 topograph of a portion of the lamella, shown in figure 8, dislocations 1 and 7 are perfectly straight ($\boldsymbol{g}.\boldsymbol{b} = 0$ for dislocations 2). Now $\boldsymbol{r}_{200}$ is [011], so the curvature of these dislocations must lie in a plane which contains [011]. Thus, the slip plane for dislocations 1 must be $(\bar{1}1\bar{1})$ and for dislocations 7 the slip plane must be $(\bar{1}\bar{1}1)$. Therefore these dislocations have not glided in the plane of the lamella, but in $\{111\}$ planes that intersect its surface. This conclusion is also indicated by stereo pairs and by the fact that intersections of these screw dislocations with the surface are generally observed. Probably they moved away from the surface. The straightness of the lines in the 200 topograph indicates that (within the resolution of this method) there is no jogging or cross slip over distances of several millimeters. This demonstration, that the screw dislocations lie exactly in the slip plane but not exacly along their Burgers vectors, and the lack of obvious sections along other $\langle 110 \rangle$ as the dislocations change from screw to edge type (see dislocations 2) argue against the importance of a Peierls force.

Dislocations 3 are hexagons lying on $(\bar{1}1\bar{1})$ with $\boldsymbol{b} = [\bar{1}01]$. Thus two sides of the hexagon are pure screw, the other four sides are 60° dislocations. As can be seen in figure 7, there are screw dislocations with $\boldsymbol{b} = [\bar{1}10]$ which are intermingled with dislocations 3. From stereo pairs it was clearly determined that the intermingling dislocations have caused the dislocations 3 to assume the hexagonal shape.

Dislocations 4 are a trace of eight dislocations which have glided on $(1\bar{1}\bar{1})$ and which intersect the (111) and $(\bar{1}\bar{1}\bar{1})$ surfaces. For them $\boldsymbol{b} = [0\bar{1}1]$ and $\boldsymbol{n} \cong [211]$; therefore they are edge dislocations. There is some curvature as they intersect both surfaces, and some anomalous contrast. Their projected length indicates a crystal thickness $\cong 0.045$ cm. Dislocations 5 are a more complicated slip trace also on $(1\bar{1}\bar{1})$ and also with $\boldsymbol{b} = [0\bar{1}1]$. There are about seventy-five dislocations in this trace, not all are parallel and not all are on the same $(1\bar{1}\bar{1})$ plane; toward the crystal edge there are two distinct rows. This trace appears to have been retarded by a few dislocations of type 1 and 7, and three dislocations at this end of the trace lean away from the remainder which are approximately parallel. For the three, $\boldsymbol{n} \cong [3\bar{4}1]$; for the remainder, $\boldsymbol{n} \cong [413]$, which is 16° from [211], the pure edge direction. Thus the three are approximately 45° dislocations.

Dislocations 6 are a group which is apparently a slip trace on $(\bar{1}1\bar{1})$ with about eleven intersections on $(\bar{1}\bar{1}\bar{1})$ but about twenty intersections on (111). It would appear that some of the dislocations are branched, but there is insufficient resolution for an unambigous determination. They are nearly pure edge dislocations with $\boldsymbol{b} = [\bar{1}10]$ and $\boldsymbol{n} = [325]$.

The availability of fresh pure screw and pure edge dislocations allows a comparison between the contrast expected and observed in a series of topographs. In Table IV are listed $|\boldsymbol{g}.\boldsymbol{b}|/|\boldsymbol{g}||\boldsymbol{b}|$ for the screw dislocations 1, 2 and 7 for a number of reflections, along with the observed contrast. Note that the observed contrast in the $1\bar{1}3$ topograph was contrary to that expected, and the added contrast expected in $0\bar{2}2$ and $20\bar{2}$ when $|\boldsymbol{g}.\boldsymbol{b}|/|\boldsymbol{g}||\boldsymbol{b}| = 1$ was not observed. There was no contrast for screw dislocations when $\boldsymbol{g}.\boldsymbol{b} = 0$, and generally there was little, if any, ano-

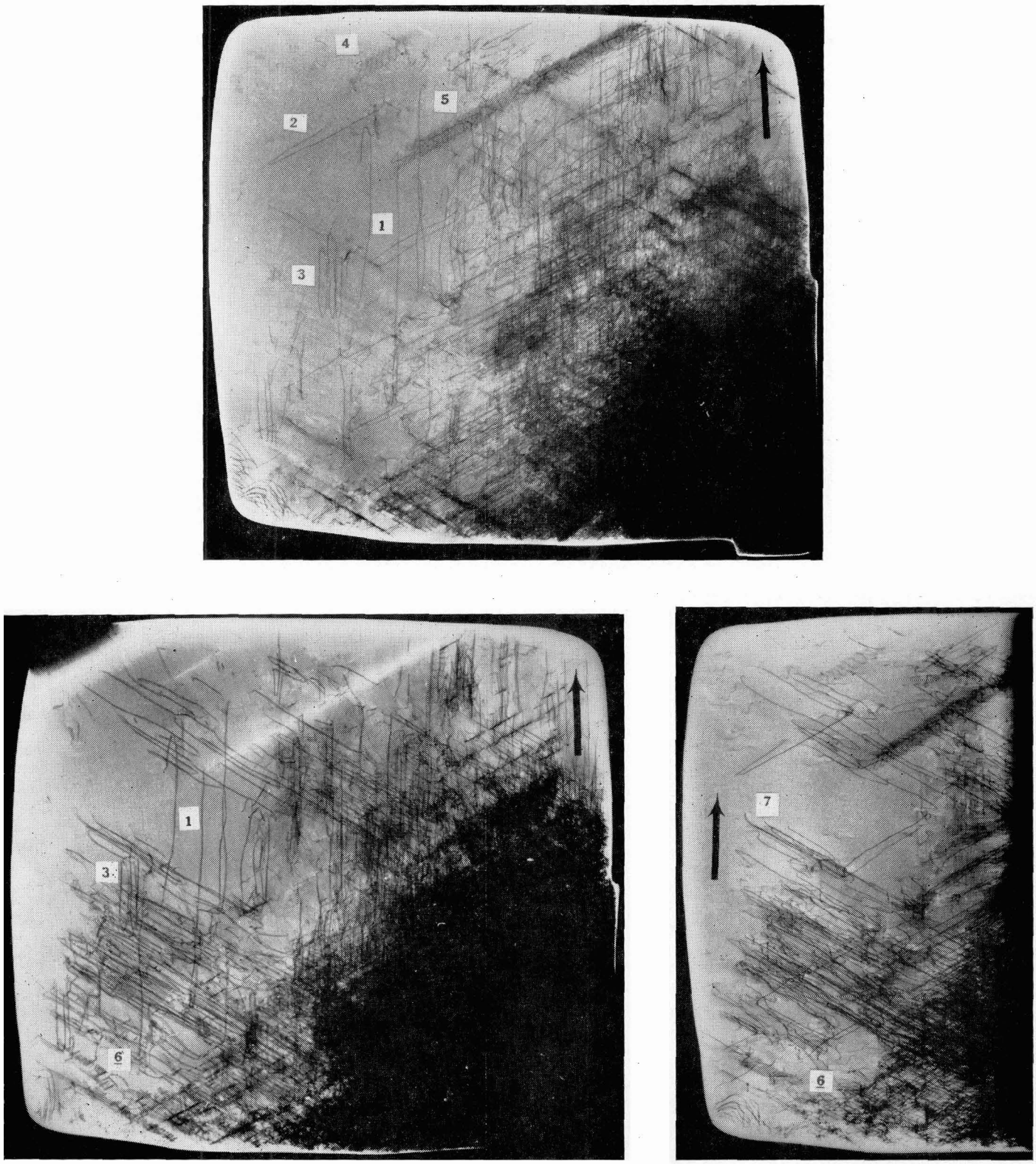

FIG. 7. — Plus topographs of the deformed lamella. *a*) $\bar{1}\bar{1}1$ Ag radiation, *b*) $1\bar{1}\bar{1}$ Mo radiation, *c*) 111 Ag radiation. Edge of lamella is 1 cm.

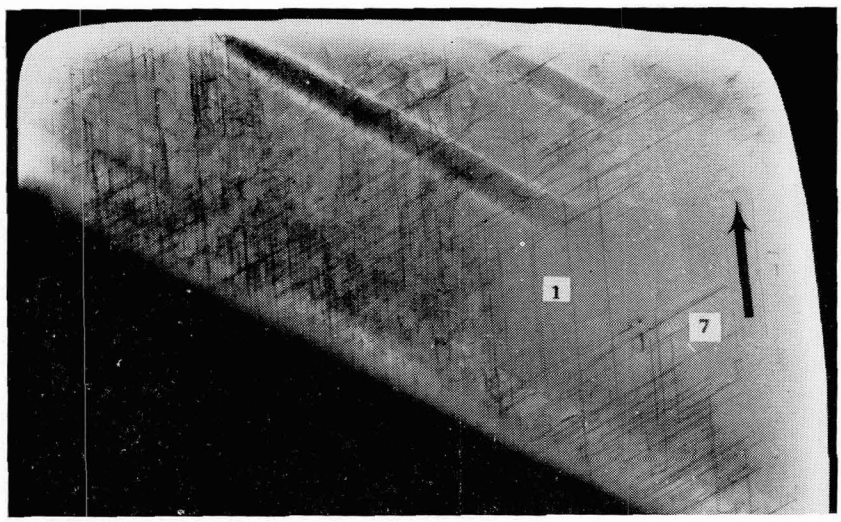

FIG. 8. — 200 minus topograph of a portion of the deformed lamella. Ag radiation.

TABLE IV

Zone	g	$\lvert g.b \rvert / \lvert g \rvert \lvert b \rvert$ (1) $\bar{1}01$	(2) $0\bar{1}1$	(7) $\bar{1}10$	Observed Contrast
—	—	—	—	—	—
	$3\bar{1}\bar{1}$	0.85	0	0.85	Dislocations 1 $\approx$ Dislocations 7
$0\bar{1}1$	022	.5	0	.5	» »
	200	.71	0	.71	» »
	$1\bar{1}\bar{1}$	.82	0	.82	» »
$2\bar{1}\bar{1}$	$0\bar{2}2$	.5	1.0	.5	Dislocations 1 $\approx$ Dislocations 7 $\gtrsim$ Dislocations 2
	$1\bar{1}3$	.43	.85	.43	Dislocations 7 has much more contrast than other two
$\bar{1}2\bar{1}$	$20\bar{2}$	1.0	.5	.5	Dislocations 7 $\approx$ Dislocations 2 $\gtrsim$ Dislocations 1
$\bar{1}01$	$\bar{1}1\bar{1}$	0	.82	.82	Dislocations 7 $\approx$ Dislocations 2
$\bar{1}10$	$\bar{1}\bar{1}1$	.82	.82	0	Dislocations 1 $\approx$ Dislocations 2

malous contrast associated with them. For edges there was some contrast in all topographs, generally anomalous contrast when $g.b = 0$. The strongest anomalous contrast was associated with the dislocations near the surfaces. However, in the 200 topograph the edge dislocations 4 appear faint with anomalous contrast although $g.b = 0$.

The widths of the images of dislocations 1, 2, 7 and 4 are listed in Table V for the same reflections as Table IV. Although the accuracy of the measurements of the image widths is not high, it is clear that the width is not a simple function of $|g.b|/|g||b|$. All image widths are smaller in the 200 topographs. The widths of dislocations 2 in $0\bar{2}2$ and dislocation 1 in $20\bar{2}$ topographs were greater than in the other topographs. These dislocations lie exactly horizontal in these topographs, there is no contribution from Borrmann delta [3] to the width, and the observed width is two to three times the vertical divergence of the instrument.

TABLE V

Zone	g	Image Width (microns) $\bar{1}01$ (1) screw	$0\bar{1}1$ (2) screw	$\bar{1}10$ (7) screw	$0\bar{1}1$ (4) edge
	$3\bar{1}\bar{1}$	14	—	12	15
	022	8	—	8	—
$0\bar{1}1$	200	7	—	7	7
	$1\bar{1}\bar{1}$	10	—	10	—
$2\bar{1}\bar{1}$	$0\bar{2}2$	10	12	10	10
	$1\bar{1}3$	11	11	14	9
$\bar{1}2\bar{1}$	$20\bar{2}$	11	10	10	—
$\bar{1}01$	$\bar{1}1\bar{1}$	—	10	10	12
$\bar{1}10$	$\bar{1}\bar{1}1$	10	12	—	9

It is apparent that although the simple rules no contrast if $\boldsymbol{g}.\boldsymbol{b} = 0$ and if $\boldsymbol{b}.(\boldsymbol{g} \times \boldsymbol{n}) = 0$ can be used to determine Burgers vectors, the magnitudes of $|\boldsymbol{g}.\boldsymbol{b}|/|\boldsymbol{g}|\,|\boldsymbol{b}|$ and for $|\boldsymbol{b}.(\boldsymbol{g} \times \boldsymbol{n})|/|\boldsymbol{g}|\,|\boldsymbol{b}|$ do not account for the details of dislocation contrast or image width. This subject is being investigated further.

Acknowledgment. — We thank F. A. Sherrill for taking many of the topographs and B. F. Day for printing. Also, we have profited greatly from discussions with D. K. Holmes, V. K. Paré and T. O. Baldwin.

Bibliographie

[1] AUTHIER (A.), ROGERS (C. B.), and LANG (A. R.), *Phil. Mag.*, 1965, **10**, 547 ; LANG (A. R.), and POLCAROVA (M.), *Proc. Roy. Soc.* A, 1965, **285**, 297 ; SAUVAGE, (M.) and AUTHIER (A.), *Bull. Soc. Franc. Miner. Crist.*, 1965, **88**, 379 ; JENKINSON (A. E.), and LANG (A. R.) in *Direct Observations of Imperfections in Crystals*, John Wiley, New York, 1962, p. 47 ; LANG (A. R.), *Encyclopedia of X-Rays and Gamma Rays*, Reinhold, New York, 1963, p. 1053.

[2] YOUNG (F. W.), Jr., SHERRILL (F. A.), and WITTELS (M. C.), *J. Appl. Phys.*, 1965, **36**, 2225.

[3] YOUNG (F. W.), Jr., BALDWIN (T. O.), MERLINI (A. E.), and SHERRILL (F. A.), *Advances in X-Ray Analysis*, Plenum Press, Vol. 9, 1966.

[4] YOUNG (F. W.), Jr., and SAVAGE (J. R.), *J. Appl. Phys.*, 1964, **35**, 1917.

[5] YOUNG (F. W.), Jr., and WILSON (T. R.), *Rev. Sci. Inst.*, 1961, **32**, 559.

[6] YOUNG (F. W.), Jr., BALDWIN (T. O.) and SHERRILL (F. A.) (in press).